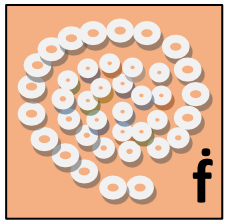

International Journal of Mathematical Analysis and Modelling

(Formerly Journal of the Nigerian Society for Mathematical Biology)

Volume 9 Issue 1 (June), 2026

ISSN (Print): 2682 - 5694
ISSN (Online): 2682 – 5708
www.tnsmb.org

Optimal control strategies for the transmission dynamics of Giardiasis

Timothy Ado Shamaki*

Abstract

This work develops and examines a deterministic mathematical model of giardiasis transmission, explicitly including the frequently neglected influence of asymptomatic carriers and the environmental pathogen reservoir. A thorough dynamical systems analysis of the autonomous model is performed, confirming the positivity and boundedness of solutions to ensure epidemiological well-posedness. We calculate the basic reproduction number ($\mathcal{R}_0$) employing the next-generation matrix approach and formally delineate the criteria for the local asymptotic stability of the disease-free equilibrium. We enhance the model by incorporating optimum control theory to meet the essential requirement for economical, time-sensitive intervention tactics. We provide three dynamic control functions that represent the medical treatment of symptomatic persons, the active screening of asymptomatic carriers, and environmental sanitation initiatives. Utilizing Pontryagin's Maximum Principle, we establish the requisite conditions for optimal control and simulate diverse intervention scenarios. Our findings demonstrate that single-intervention methods achieve limited efficacy, but a multifaceted, integrated strategy substantially reduces both the human disease burden and environmental pollution. Moreover, we illustrate that a focused strategy integrating immediate treatment with proactive asymptomatic screening provides a highly cost-effective option for resource-limited environments. This study offers substantial mathematical insights and a quantitative public health framework for the development of effective and sustainable giardiasis control initiatives.

Keywords and phrases: Giardiasis; compartmental model; stability analysis; optimal control; forward-backward sweep method.

1 Introduction

Giardiasis, caused by the protozoan parasite *Giardia duodenalis*, remains a persistent and pervasive global public health threat. People in low- and middle-income countries (LMICs), where access to clean water, sanitation, and hygiene (WASH) infrastructure is essentially insufficient, are disproportionately affected [1, 2, 3]. As a leading cause of diarrheal disease globally, giardiasis contributes heavily to acute morbidity, severe malnutrition, stunted growth in children, and long-term cognitive impairment, thereby perpetuating vicious cycles of poverty and ill-health [4, 5]. Through its Neglected Diseases Initiative, the World Health Organization (WHO) officially designated giardiasis as a neglected tropical disease (NTD) due to its significant socioeconomic impact [5, 6], underscoring the urgent need for enhanced, sustainable control strategies to meet eradication benchmarks established for 2030 [7].

The epidemiological dynamics of *Giardia* are exceedingly complex. Transmission occurs predominantly via the fecal-oral pathway, induced either by the consumption of infectious cysts from contaminated water and food or through direct person-to-person contact [8, 9]. Effectively curtailing giardiasis is fundamentally challenged by the triad of its transmission network: symptomatic individuals who actively shed the pathogen, environmental reservoirs where cysts can survive for months under harsh conditions [3], and asymptomatic carriers. Asymptomatic individuals show no overt clinical signs yet

*E-mail: tashamaki.math@futb.edu.ng; Department of Applied Mathematics, Federal University of Technology Babura, Jigawa State, Nigeria

shed large volumes of cysts over extended periods [4]. This makes them a "silent" reservoir that effectively sustains community spread and continuously replenishes environmental contamination, severely frustrating traditional intervention methods [32, 33, 34, 35].

To fully understand and predict the spread of such complicated diseases, mathematical modeling has shown to be a crucial theoretical tool [10, 11]. The mathematical foundation for analyzing multiple transmission pathways (e.g., human-to-human versus environment-to-human) has been well-established in the literature, particularly for severe waterborne diseases like cholera [12, 13, 14]. Advancing this methodology specifically for giardiasis, Liana and Chuma [15] recently made a valuable contribution by developing a deterministic compartmental model that explicitly incorporated the oft-neglected role of asymptomatic carriers. Employing the next-generation matrix method [16], their static sensitivity analysis showed that the fundamental reproduction number ($\mathcal{R}_0$) is significantly influenced by characteristics related to treatment, screening, and cleanliness, theoretically proving the necessity of a multi-pronged intervention approach.

However, a major limitation in the existing giardiasis modeling literature—including the foundational work by Liana and Chuma [15]—is the reliance on constant, static control parameters. In realistic public health scenarios, financial and logistical resources are strictly constrained. Thus, the intensity of interventions cannot remain constant; it must adapt dynamically to the evolving epidemiological burden and shifting budgetary realities [17, 18].

To bridge the gap between theoretical disease modeling and actionable public policy, optimal control theory offers a highly robust mathematical framework. Founded on Pontryagin's Maximum Principle [19, 20, 21], optimum control permits researchers to build time-dependent intervention profiles that actively decrease both the burden of disease and the related economic costs. In recent years, this mathematical methodology has been successfully deployed to optimize resource allocation for numerous infectious diseases, including malaria [22, 23], cholera [24, 25], Ebola [26], tuberculosis [27], and various vector-borne illnesses [28, 29].

Despite these broad advancements across mathematical epidemiology, the application of dynamic optimal control specifically to the complex transmission tripartite of giardiasis remains largely unexplored. This paper seeks to rigorously fill this critical gap. First, we rigorously establish the epidemiological well-posedness of the giardiasis transmission model by proving the positivity and boundedness of its solutions, a crucial dynamical systems analysis step often omitted in applied control studies [11]. We subsequently derive $\mathcal{R}_0$ [30] and establish the stability of the disease-free equilibrium. Building on this sound mathematical foundation, we formulate an optimal control problem featuring three dynamic control variables: the medical treatment of symptomatic individuals, the active surveillance of asymptomatic carriers, and environmental sanitation. By solving this system numerically, we provide a mathematically rigorous, cost-effective framework that precisely guides *when* and *how intensely* public health resources should be deployed to eradicate a giardiasis outbreak.

2 Model Formulation

We explore a deterministic compartmental model for giardiasis transmission in a homogeneously mixed human population, together with an environmental pathogen compartment. The complete human population $N(t)$ is divided into five mutually exclusive compartments: susceptible (S), exposed/latent (E), symptomatic infectious (I), asymptomatic carriers (A), and recovered/immune (R). $G(t)$ represents the concentration of *Giardia* cysts in the environment.

The baseline autonomous transmission model is governed by the following system of non-linear

ordinary differential equations:

$$\frac{dS}{dt} = \Lambda + \rho R - \lambda(t)S - \mu S \tag{1}$$
$$\frac{dE}{dt} = \lambda(t)S - (\mu + \kappa)E \tag{2}$$
$$\frac{dI}{dt} = (1-\alpha)\kappa E - (\eta + \psi + \mu + p)I \tag{3}$$
$$\frac{dA}{dt} = \alpha\kappa E + \eta I - (\mu + \gamma)A \tag{4}$$
$$\frac{dR}{dt} = pI + \gamma A - (\mu + \rho)R \tag{5}$$
$$\frac{dG}{dt} = \varepsilon I + dA - \tau G \tag{6}$$

Here, the force of infection is defined as $\lambda(t) = \beta_1 I(t) + \beta_2 A(t) + \beta_3 G(t)$, reflecting transmission via contact with symptomatic individuals, asymptomatic individuals, and the contaminated environment, respectively. Susceptible individuals are recruited at a steady pace Λ. Natural mortality occurs in all human compartments at a rate μ, while disease-induced death occurs in the symptomatic class at a rate ψ. Exposed people move to the infectious stage at a rate κ, where a proportion $(1-\alpha)$ becomes symptomatic (I) and a proportion α becomes asymptomatic (A). Symptomatic individuals may advance to an asymptomatic carrier state at a rate η, or spontaneously recover at a rate p. Asymptomatic carriers recover spontaneously at a rate γ. Recovered individuals lose their temporary immunity at a rate ρ, returning to the susceptible class. Pathogens are shed into the environment by symptomatic and asymptomatic persons at rates ε and d, respectively, and decay naturally at a rate τ.

Table 1 provides a summary of the nominal parameter values used in our analysis and numerical simulations.

Table 1: Epidemiological parameter descriptions and nominal baseline values.

Parameter	Description	Nominal Value	Source/Reference
Λ	Human population recruitment rate	100 day^{-1}	Assumed
β_1	Direct transmission rate (symptomatic)	2.5×10^{-4} day^{-1}	[15]
β_2	Direct transmission rate (asymptomatic)	1.2×10^{-4} day^{-1}	[15]
β_3	Indirect environmental transmission rate	1.5×10^{-5} day^{-1}	[9]
μ	Natural human mortality rate	4.5×10^{-5} day^{-1}	WHO Cohort
κ	Progression rate from exposed to active	0.142 day^{-1}	[2]
$1-\alpha$	Proportion remaining symptomatic	0.35	[33]
η	Symptomatic transition rate to carrier	0.05 day^{-1}	Assumed
ψ	Disease-induced human mortality rate	1.0×10^{-3} day^{-1}	Clinical Est.
p	Spontaneous recovery (symptomatic)	0.07 day^{-1}	[31]
γ	Spontaneous recovery (asymptomatic)	0.04 day^{-1}	[33]
ρ	Loss of temporary acquired immunity	0.01 day^{-1}	[23]
ε	Pathogen shedding rate (symptomatic)	1.5 day^{-1}	[15]
d	Pathogen shedding rate (asymptomatic)	0.8 day^{-1}	[15]
τ	Natural environmental pathogen decay rate	0.035 day^{-1}	[9]

3 Analysis of the Model

In this section, we analyze the qualitative dynamics of the uncontrolled system (1)–(6). Before establishing equilibria, we must rigorously prove that the model is epidemiologically well-posed by showing that its solutions remain non-negative and bounded for all $t \geq 0$.

3.1 Positivity of Solutions

Since the model tracks physical human populations and environmental pathogen concentrations, all state variables must remain non-negative given non-negative initial conditions.

Theorem 3.1 (Positivity). *Let the initial data be* $S(0) \geq 0, E(0) \geq 0, I(0) \geq 0, A(0) \geq 0, R(0) \geq 0,$ *and* $G(0) \geq 0$. *Then the solutions* $(S(t), E(t), I(t), A(t), R(t), G(t))$ *of the system* (1)–(6) *are positive for all* $t > 0$.

Proof. Consider the equations sequentially. From equation (1), we can express the rate of change as:

$$\frac{dS}{dt} + (\lambda(t) + \mu)S = \Lambda + \rho R$$

Using an integrating factor $M(t) = \exp\left(\int_0^t (\lambda(s) + \mu)ds\right)$, this can be integrated explicitly:

$$S(t) = S(0)e^{-\int_0^t (\lambda(s)+\mu)ds} + \int_0^t (\Lambda + \rho R(\xi))e^{-\int_\xi^t (\lambda(s)+\mu)ds} d\xi$$

Since $\Lambda > 0$ and the exponential function is strictly positive, it follows that if $S(0) \geq 0$ and $R(t) \geq 0$, then $S(t) > 0$ for all $t > 0$.

For the remaining boundaries of the non-negative cone $\mathbb{R}^6_+$, we evaluate the vector field directly on each boundary plane:

$$\begin{aligned}
\left.\frac{dE}{dt}\right|_{E=0} &= \lambda(t)S = (\beta_1 I + \beta_2 A + \beta_3 G)S \geq 0 \quad \text{for } S, I, A, G \geq 0, \\
\left.\frac{dI}{dt}\right|_{I=0} &= (1-\alpha)\kappa E \geq 0 \quad \text{for } E \geq 0, \\
\left.\frac{dA}{dt}\right|_{A=0} &= \alpha\kappa E + \eta I \geq 0 \quad \text{for } E, I \geq 0, \\
\left.\frac{dR}{dt}\right|_{R=0} &= pI + \gamma A \geq 0 \quad \text{for } I, A \geq 0, \\
\left.\frac{dG}{dt}\right|_{G=0} &= \varepsilon I + dA \geq 0 \quad \text{for } I, A \geq 0.
\end{aligned}$$

Since all rates of change are strictly non-negative on the boundary planes, any solution trajectory starting within $\mathbb{R}^6_+$ can never cross the boundaries. By standard differential equations theory, the solutions remain entirely in $\mathbb{R}^6_+$ for all $t > 0$. □

3.2 Boundedness of Solutions

We must also demonstrate that the population and pathogen levels do not grow infinitely, ensuring the system remains biologically realistic over time.

Theorem 3.2 (Boundedness). *All solutions of the system* (1)–(6) *starting in* $\mathbb{R}^6_+$ *are bounded, and there exists a positively invariant region* Ω *such that all solutions eventually enter and remain in* Ω.

Proof. Let $N(t) = S(t) + E(t) + I(t) + A(t) + R(t)$ represent the total human population size. Summing equations (1) through (5) gives the rate of change of the total population:

$$\frac{dN}{dt} = \Lambda - \mu N - \psi I$$

Since disease-induced death $\psi I \geq 0$ due to the positivity of solutions, it follows that:

$$\frac{dN}{dt} \leq \Lambda - \mu N$$

Integrating this differential inequality via an integrating factor yields:

$$N(t) \leq N(0)e^{-\mu t} + \frac{\Lambda}{\mu}\left(1 - e^{-\mu t}\right)$$

Taking the supremum limit as $t \to \infty$, we obtain $\limsup_{t\to\infty} N(t) \leq \frac{\Lambda}{\mu}$. Thus, the human population size is strictly bounded above.

For the environmental pathogen compartment, equation (6) dictates:

$$\frac{dG}{dt} = \varepsilon I + dA - \tau G$$

Since $I(t) \leq N(t)$ and $A(t) \leq N(t)$, we can establish a differential upper bound using the human population carrying capacity:

$$\frac{dG}{dt} \leq (\varepsilon + d)N(t) - \tau G \leq (\varepsilon + d)\frac{\Lambda}{\mu} - \tau G$$

Applying standard comparison theorems results in:

$$G(t) \leq G(0)e^{-\tau t} + \frac{(\varepsilon + d)\Lambda}{\mu\tau}\left(1 - e^{-\tau t}\right)$$

Consequently, taking the limit yields:

$$\limsup_{t\to\infty} G(t) \leq \frac{(\varepsilon + d)\Lambda}{\mu\tau}$$

Hence, all state solutions are bounded, and the biologically feasible region defined by:

$$\Omega = \left\{(S, E, I, A, R, G) \in \mathbb{R}^6_+ : N \leq \frac{\Lambda}{\mu}, G \leq \frac{(\varepsilon + d)\Lambda}{\mu\tau}\right\}$$

is epidemiologically well-posed, positively invariant, and attracting. □

3.3 Disease-Free Equilibrium (DFE)

The disease-free equilibrium (DFE), denoted by $\mathcal{E}_0$, is the steady-state solution wherein the pathogen is completely eradicated from both the population and the environment. Setting the time derivatives in equations (1)–(6) to zero and substituting $E = I = A = G = 0$, we obtain:

$$\mathcal{E}_0 = (S^0, E^0, I^0, A^0, R^0, G^0) = \left(\frac{\Lambda}{\mu}, 0, 0, 0, 0, 0\right) \tag{7}$$

3.4 Basic Reproduction Number ($\mathcal{R}_0$)

The basic reproduction number, $\mathcal{R}_0$, represents the expected number of secondary cases produced by a single typical infected individual entering a completely susceptible population. We derive $\mathcal{R}_0$ utilizing the next-generation matrix method formulated by van den Driessche and Watmough [30].

The infected and infectious compartments are E, I, A, and G. Let $\mathcal{F}$ represent the rate of appearance of new infections into these compartments, and let $\mathcal{V}$ represent the rate of other transitions (transfers in and out). We define:

$$\mathcal{F} = \begin{bmatrix} (\beta_1 I + \beta_2 A + \beta_3 G)S \\ 0 \\ 0 \\ 0 \end{bmatrix}, \quad \mathcal{V} = \begin{bmatrix} (\mu + \kappa)E \\ -(1-\alpha)\kappa E + (\eta + \psi + \mu + p)I \\ -\alpha\kappa E - \eta I + (\mu + \gamma)A \\ -\varepsilon I - dA + \tau G \end{bmatrix} \tag{8}$$

To simplify notation, let us define the rate constants representing the total removal rates from their respective compartments: $k_1 = \mu + \kappa, \quad k_2 = \eta + \psi + \mu + p, \quad k_3 = \mu + \gamma, \quad k_4 = \tau.$

The Jacobian matrices F and V, evaluated at the DFE $\mathcal{E}_0$, are constructed as:

$$F = \begin{bmatrix} 0 & \beta_1 S^0 & \beta_2 S^0 & \beta_3 S^0 \\ 0 & 0 & 0 & 0 \\ 0 & 0 & 0 & 0 \\ 0 & 0 & 0 & 0 \end{bmatrix}, \quad V = \begin{bmatrix} k_1 & 0 & 0 & 0 \\ -(1-\alpha)\kappa & k_2 & 0 & 0 \\ -\alpha\kappa & -\eta & k_3 & 0 \\ 0 & -\varepsilon & -d & k_4 \end{bmatrix} \tag{9}$$

The basic reproduction number $\mathcal{R}_0$ is defined mathematically as the spectral radius (the dominant eigenvalue) of the next-generation matrix FV^{-1}. Computing the inverse matrix V^{-1} explicitly yields:

$$V^{-1} = \begin{bmatrix} \frac{1}{k_1} & 0 & 0 & 0 \\ \frac{(1-\alpha)\kappa}{k_1 k_2} & \frac{1}{k_2} & 0 & 0 \\ \frac{\kappa[\alpha k_2 + \eta(1-\alpha)]}{k_1 k_2 k_3} & \frac{\eta}{k_2 k_3} & \frac{1}{k_3} & 0 \\ \frac{\kappa[\varepsilon k_3(1-\alpha) + d\alpha k_2 + d\eta(1-\alpha)]}{k_1 k_2 k_3 k_4} & \frac{\varepsilon k_3 + d\eta}{k_2 k_3 k_4} & \frac{d}{k_3 k_4} & \frac{1}{k_4} \end{bmatrix} \tag{10}$$

Finding the spectral radius $\rho(FV^{-1})$ provides the explicit analytical expression:

$$\mathcal{R}_0 = \frac{\Lambda}{\mu k_1}\left[(1-\alpha)\kappa\left(\frac{\beta_1}{k_2} + \frac{\eta\beta_2}{k_2 k_3} + \frac{\beta_3}{k_2 k_4}\left(\varepsilon + \frac{\eta d}{k_3}\right)\right) + \alpha\kappa\left(\frac{\beta_2}{k_3} + \frac{\beta_3 d}{k_3 k_4}\right)\right] \tag{11}$$

The expression derived in (11) represents the cumulative sum of new infections generated across all specific biological pathways: direct transmission from acute symptomatic cases, direct transmission from asymptomatic cases, and indirect transmission stemming from the environmental shedding of both human cohorts.

3.5 Local Stability of the Disease-Free Equilibrium

Theorem 3.3. *The disease-free equilibrium $\mathcal{E}_0$ of the giardiasis model is locally asymptotically stable if $\mathcal{R}_0 < 1$, and unstable if $\mathcal{R}_0 > 1$.*

Proof. To formally determine the local stability of the DFE, we construct the Jacobian matrix J of the full system (1)–(6) evaluated at $\mathcal{E}_0$. Let $k_5 = \mu + \rho$ denote the total removal rate from the recovered class. The 6×6 Jacobian matrix at the DFE is explicitly given by:

$$J(\mathcal{E}_0) = \begin{bmatrix} -\mu & 0 & -\beta_1 S^0 & -\beta_2 S^0 & \rho & -\beta_3 S^0 \\ 0 & -k_1 & \beta_1 S^0 & \beta_2 S^0 & 0 & \beta_3 S^0 \\ 0 & (1-\alpha)\kappa & -k_2 & 0 & 0 & 0 \\ 0 & \alpha\kappa & \eta & -k_3 & 0 & 0 \\ 0 & 0 & p & \gamma & -k_5 & 0 \\ 0 & 0 & \varepsilon & d & 0 & -k_4 \end{bmatrix} \tag{12}$$

By rearranging the order of the state variables to separate the uninfected compartments (S, R) from the infected compartments (E, I, A, G), the Jacobian matrix transforms into a block upper-triangular form:

$$J^*(\mathcal{E}_0) = \begin{bmatrix} -\mu & \rho & 0 & -\beta_1 S^0 & -\beta_2 S^0 & -\beta_3 S^0 \\ 0 & -k_5 & 0 & p & \gamma & 0 \\ 0 & 0 & -k_1 & \beta_1 S^0 & \beta_2 S^0 & \beta_3 S^0 \\ 0 & 0 & (1-\alpha)\kappa & -k_2 & 0 & 0 \\ 0 & 0 & \alpha\kappa & \eta & -k_3 & 0 \\ 0 & 0 & 0 & \varepsilon & d & -k_4 \end{bmatrix} = \begin{bmatrix} J_1 & J_{12} \\ 0 & J_2 \end{bmatrix} \tag{13}$$

Because of this distinct block upper-triangular structure, the eigenvalues of $J(\mathcal{E}_0)$ are simply the union of the eigenvalues of the independent diagonal submatrices J_1 and J_2.

The upper 2×2 submatrix J_1 is:

$$J_1 = \begin{bmatrix} -\mu & \rho \\ 0 & -k_5 \end{bmatrix}$$

which immediately yields two strictly negative eigenvalues: $\lambda_1 = -\mu$ and $\lambda_2 = -k_5 = -(\mu + \rho)$.

The remaining lower 4×4 submatrix J_2, which thoroughly governs the dynamics of the infected compartments, corresponds exactly to the matrix $F - V$ derived earlier via the next-generation matrix method:

$$J_2 = F - V = \begin{bmatrix} -k_1 & \beta_1 S^0 & \beta_2 S^0 & \beta_3 S^0 \\ (1-\alpha)\kappa & -k_2 & 0 & 0 \\ \alpha\kappa & \eta & -k_3 & 0 \\ 0 & \varepsilon & d & -k_4 \end{bmatrix}$$

According to the fundamental properties of next-generation matrix theory [30], since F is a non-negative matrix and V is a non-singular M-matrix, all eigenvalues of the matrix $J_2 = F - V$ have strictly negative real parts if and only if the spectral radius $\rho(FV^{-1}) < 1$.

Because we have mathematically defined $\mathcal{R}_0 = \rho(FV^{-1})$, it follows conclusively that when $\mathcal{R}_0 < 1$, all six eigenvalues of the full Jacobian matrix $J(\mathcal{E}_0)$ possess strictly negative real parts. This guarantees that the DFE is locally asymptotically stable. If $\mathcal{R}_0 > 1$, J_2 contains at least one eigenvalue with a positive real part, rendering the DFE unstable. □

4 Optimal Control Model Formulation

To actively drive the dynamical system toward disease eradication while simultaneously minimizing economic constraints, we extend the autonomous system into an optimal control framework. We introduce three time-dependent control variables, each bounded between 0 and a realistic maximum feasible capacity $u_{k,\max}$:

- $u_1(t)$: Effort for the medical treatment of symptomatic individuals ($0 \leq u_1(t) \leq u_{1,\max}$). This public health control represents the direct allocation of clinical resources, diagnostic clinics, and anti-parasitic therapeutics.
- $u_2(t)$: Effort for the active screening, identification, and subsequent treatment of asymptomatic carriers ($0 \leq u_2(t) \leq u_{2,\max}$). This represents community-based diagnostic test deployment and active surveillance.
- $u_3(t)$: Environmental sanitation effort ($0 \leq u_3(t) \leq u_{3,\max}$). This control represents broad WASH interventions aimed at clearing environmental cysts, such as enhanced water chlorination, filtration, and improved sewage infrastructure.

Incorporating these dynamic controls modifies the state equations as follows:

$$\frac{dS}{dt} = \Lambda + \rho R - (\beta_1 I + \beta_2 A + \beta_3 G)S - \mu S \tag{14}$$

$$\frac{dE}{dt} = (\beta_1 I + \beta_2 A + \beta_3 G)S - (\mu + \kappa)E \tag{15}$$

$$\frac{dI}{dt} = (1-\alpha)\kappa E + u_2(t)A - (\eta + \psi + \mu + p + u_1(t))I \tag{16}$$

$$\frac{dA}{dt} = \alpha\kappa E + \eta I - (\mu + u_2(t) + \gamma)A \tag{17}$$

$$\frac{dR}{dt} = (p + u_1(t))I + \gamma A - (\mu + \rho)R \tag{18}$$

$$\frac{dG}{dt} = \varepsilon I + dA - (\tau + u_3(t))G \tag{19}$$

Epidemiologically, the control $u_1(t)$ directly increases the rate at which symptomatic individuals transition to the recovered class. The control $u_2(t)$ actively removes individuals from the asymptomatic reservoir, shifting them to the treated track via coordinated state-to-control coupling. Finally, the control $u_3(t)$ acts as an additive decay rate on environmental pathogens.

The objective is to minimize the human disease burden (both symptomatic and asymptomatic cases), the environmental contamination level, and the economic costs of implementing the controls over a given time horizon $[0, T_f]$. We define the objective functional J as:

$$J(u_1, u_2, u_3) = \int_0^{T_f} \left[W_1 I(t) + W_2 A(t) + W_3 G(t) + \frac{B_1}{2} u_1^2(t) + \frac{B_2}{2} u_2^2(t) + \frac{B_3}{2} u_3^2(t) \right] dt \quad (20)$$

where W_1, W_2, W_3 are positive weight constants prioritizing the minimization of the state variables I, A, and G respectively, and B_1, B_2, B_3 represent the relative economic costs associated with implementing the controls. The quadratic cost terms $\frac{B_k}{2} u_k^2(t)$ are standard constructs in optimal control [21], utilized to reflect the non-linear scaling of costs (i.e., the marginal cost of an intervention increases significantly at high implementation intensities due to supply chain stress and diminishing returns).

5 Application of Pontryagin's Maximum Principle

To find the optimal control set $u^*(t) = (u_1^*(t), u_2^*(t), u_3^*(t))$ that minimizes the cost functional $J(u_1, u_2, u_3)$ subject to the state system (14)–(19), we utilize Pontryagin's Maximum Principle [19, 21]. This principle transforms the problem of minimizing the integral functional into the problem of minimizing the Hamiltonian $\mathcal{H}$ pointwise with respect to the controls.

We define the Hamiltonian $\mathcal{H}$ by adjoining the continuous state equations to the objective integrand via the adjoint (co-state) variables $\lambda_X(t)$ corresponding to each state variable $X \in \{S, E, I, A, R, G\}$:

$$\begin{aligned} \mathcal{H} = {} & W_1 I + W_2 A + W_3 G + \frac{B_1}{2} u_1^2 + \frac{B_2}{2} u_2^2 + \frac{B_3}{2} u_3^2 \\ & + \lambda_S \left[\Lambda + \rho R - (\beta_1 I + \beta_2 A + \beta_3 G) S - \mu S \right] \\ & + \lambda_E \left[(\beta_1 I + \beta_2 A + \beta_3 G) S - (\mu + \kappa) E \right] \\ & + \lambda_I \left[(1 - \alpha)\kappa E + u_2 A - (\eta + \psi + \mu + p + u_1) I \right] \\ & + \lambda_A \left[\alpha\kappa E + \eta I - (\mu + u_2 + \gamma) A \right] \\ & + \lambda_R \left[(p + u_1) I + \gamma A - (\mu + \rho) R \right] \\ & + \lambda_G \left[\varepsilon I + dA - (\tau + u_3) G \right] \end{aligned} \quad (21)$$

Given optimal controls u_1^*, u_2^*, u_3^* and the corresponding state solutions S, E, I, A, R, G of the controlled system (14)–(19), there exist adjoint variables $\lambda_S(t), \lambda_E(t), \lambda_I(t), \lambda_A(t), \lambda_R(t), \lambda_G(t)$ satisfying the adjoint differential system:

$$\frac{d\lambda_S}{dt} = (\lambda_S - \lambda_E)(\beta_1 I + \beta_2 A + \beta_3 G) + \lambda_S \mu \quad (22)$$

$$\frac{d\lambda_E}{dt} = \lambda_E(\mu + \kappa) - \lambda_I(1 - \alpha)\kappa - \lambda_A \alpha\kappa \quad (23)$$

$$\frac{d\lambda_I}{dt} = -W_1 + (\lambda_S - \lambda_E)\beta_1 S + \lambda_I(\eta + \psi + \mu + p + u_1(t)) - \lambda_A \eta - \lambda_R(p + u_1(t)) - \lambda_G \varepsilon \quad (24)$$

$$\frac{d\lambda_A}{dt} = -W_2 + (\lambda_S - \lambda_E)\beta_2 S - \lambda_I u_2(t) + \lambda_A(\mu + u_2(t) + \gamma) - \lambda_R \gamma - \lambda_G d \quad (25)$$

$$\frac{d\lambda_R}{dt} = -\lambda_S \rho + \lambda_R(\mu + \rho) \quad (26)$$

$$\frac{d\lambda_G}{dt} = -W_3 + (\lambda_S - \lambda_E)\beta_3 S + \lambda_G(\tau + u_3(t)) \quad (27)$$

with transversality conditions defined as $\lambda_X(T_f) = 0$ for all $X \in \{S, E, I, A, R, G\}$.

Furthermore, the optimal controls $u_k^*(t)$ are mathematically characterized by the piecewise functions:

$$u_1^*(t) = \max\left\{0, \min\left\{u_{1,\max}, \frac{(\lambda_I(t) - \lambda_R(t))I(t)}{B_1}\right\}\right\} \tag{28}$$

$$u_2^*(t) = \max\left\{0, \min\left\{u_{2,\max}, \frac{(\lambda_A(t) - \lambda_I(t))A(t)}{B_2}\right\}\right\} \tag{29}$$

$$u_3^*(t) = \max\left\{0, \min\left\{u_{3,\max}, \frac{\lambda_G(t)G(t)}{B_3}\right\}\right\} \tag{30}$$

Proof. By Pontryagin's Maximum Principle, the adjoint equations are obtained strictly by taking the negative partial derivatives of the Hamiltonian (21) with respect to each corresponding state variable: $\frac{d\lambda_X}{dt} = -\frac{\partial \mathcal{H}}{\partial X}$.

For the Susceptible (S) compartment:

$$\begin{aligned}\frac{d\lambda_S}{dt} &= -\frac{\partial \mathcal{H}}{\partial S} = -\left[\lambda_S(-(\beta_1 I + \beta_2 A + \beta_3 G) - \mu) + \lambda_E(\beta_1 I + \beta_2 A + \beta_3 G)\right] \\ &= (\lambda_S - \lambda_E)(\beta_1 I + \beta_2 A + \beta_3 G) + \lambda_S \mu\end{aligned}$$

For the Exposed (E) compartment:

$$\begin{aligned}\frac{d\lambda_E}{dt} &= -\frac{\partial \mathcal{H}}{\partial E} = -\left[-\lambda_E(\mu + \kappa) + \lambda_I(1-\alpha)\kappa + \lambda_A \alpha \kappa\right] \\ &= \lambda_E(\mu + \kappa) - \lambda_I(1-\alpha)\kappa - \lambda_A \alpha \kappa\end{aligned}$$

For the Symptomatic Infectious (I) compartment:

$$\begin{aligned}\frac{d\lambda_I}{dt} &= -\frac{\partial \mathcal{H}}{\partial I} = -\left[W_1 - \lambda_S \beta_1 S + \lambda_E \beta_1 S - \lambda_I(\eta + \psi + \mu + p + u_1) + \lambda_A \eta + \lambda_R(p + u_1) + \lambda_G \varepsilon\right] \\ &= -W_1 + (\lambda_S - \lambda_E)\beta_1 S + \lambda_I(\eta + \psi + \mu + p + u_1) - \lambda_A \eta - \lambda_R(p + u_1) - \lambda_G \varepsilon\end{aligned}$$

For the Asymptomatic Carrier (A) compartment:

$$\begin{aligned}\frac{d\lambda_A}{dt} &= -\frac{\partial \mathcal{H}}{\partial A} = -\left[W_2 - \lambda_S \beta_2 S + \lambda_E \beta_2 S + \lambda_I u_2 - \lambda_A(\mu + u_2 + \gamma) + \lambda_R \gamma + \lambda_G d\right] \\ &= -W_2 + (\lambda_S - \lambda_E)\beta_2 S - \lambda_I u_2 + \lambda_A(\mu + u_2 + \gamma) - \lambda_R \gamma - \lambda_G d\end{aligned}$$

For the Recovered (R) compartment:

$$\frac{d\lambda_R}{dt} = -\frac{\partial \mathcal{H}}{\partial R} = -\left[\lambda_S \rho - \lambda_R(\mu + \rho)\right] = -\lambda_S \rho + \lambda_R(\mu + \rho)$$

For the Environmental Pathogen (G) compartment:

$$\begin{aligned}\frac{d\lambda_G}{dt} &= -\frac{\partial \mathcal{H}}{\partial G} = -\left[W_3 - \lambda_S \beta_3 S + \lambda_E \beta_3 S - \lambda_G(\tau + u_3)\right] \\ &= -W_3 + (\lambda_S - \lambda_E)\beta_3 S + \lambda_G(\tau + u_3)\end{aligned}$$

Because our economic problem design assumes zero terminal salvage costs, liquidation benefits, or structural scrap value accumulated at the termination boundary T_f, the terminal conditions for the unaugmented scalar Hamiltonian must reflect an unconstrained final state space. Standard optimal control theory dictates that these transversality equations evaluate directly to zero across the entire coordinate grid; thus, $\lambda_X(T_f) = 0$ holds identically for all state indices.

To mathematically deduce the explicit characterization of the control profiles, we apply the optimality condition, which requires minimizing the Hamiltonian with respect to the controls on the interior of the permissible control set. We calculate the partial derivatives $\frac{\partial \mathcal{H}}{\partial u_k}$ and equate them to zero:

$$\begin{aligned}
\frac{\partial \mathcal{H}}{\partial u_1} &= B_1 u_1 - \lambda_I I + \lambda_R I = 0 \quad \Longrightarrow \quad \tilde{u}_1 = \frac{(\lambda_I - \lambda_R) I}{B_1} \\
\frac{\partial \mathcal{H}}{\partial u_2} &= B_2 u_2 + \lambda_I A - \lambda_A A = 0 \quad \Longrightarrow \quad \tilde{u}_2 = \frac{(\lambda_A - \lambda_I) A}{B_2} \\
\frac{\partial \mathcal{H}}{\partial u_3} &= B_3 u_3 - \lambda_G G = 0 \quad \Longrightarrow \quad \tilde{u}_3 = \frac{\lambda_G G}{B_3}
\end{aligned}$$

Because the controls are bounded by minimum and maximum capacities (i.e., $0 \leq u_k \leq u_{k,\max}$), the optimal controls are constrained. Using standard projection arguments onto the feasible control space, the optimal solutions are expressed piece-wise as $u_k^*(t) = \min\{\max\{0, \tilde{u}_k\}, u_{k,\max}\}$. This definitively yields the final control characterizations in equations (28)–(30).

6 Numerical Simulations

The complete optimal control system—consisting of the state and adjoint systems along with the control characterizations—constitutes a complex two-point boundary value problem. We solve this system numerically using the well-established Forward-Backward Sweep Method (FBSM) over a designated simulation period of $T_f = 300$ days [21].

The iterative framework of the FBSM operates via the following continuous sequence:

1. Initialize a baseline piecewise profile for all time-varying control vectors $u_i(t)$ across the discretized temporal grid $[0, T_f]$.

2. Incorporating the defined initial boundary values, integrate the non-linear state ODE layout forward in time from $t = 0$ to $t = T_f$ using a 4th-order Runge-Kutta integration scheme.

3. Utilizing the resulting forward state trajectories and the zero-terminal transversality constraints ($\lambda_i(T_f) = 0$), integrate the adjoint ODE equations backward in time from $t = T_f$ to $t = 0$.

4. Update the continuous control values point-wise by inserting the current state vectors and adjoint variables into the projection optimality conditions.

5. Repeat the iteration loop until the relative absolute differences between all successive state, adjoint, and control matrices meet a strict convergence tolerance threshold of $\delta \leq 10^{-6}$.

We model an initial human population of $N = 50,000$ individuals, with initial conditions deliberately set to represent the emergence of an aggressive outbreak: $S(0) = 49,900$, $E(0) = 50$, $I(0) = 30$, $A(0) = 20$, $R(0) = 0$, and an initial environmental load $G(0) = 10$.

6.1 Parameter Justification and Optimization Weights

To strictly ensure the biological and epidemiological validity of the simulated outcomes, parameter values were sourced from established giardiasis and waterborne pathogen literature. Baseline epidemiological parameters are derived primarily from the core static model by Liana and Chuma [15], augmented where necessary by general parameters standard for neglected enteric protozoan infections [35, 9].

Rather than choosing arbitrary values, the optimization weights (W_i, B_i) and maximum control bounds ($u_{i,\max}$) are explicitly calibrated to reflect real-world public health operational matrices and relative economic scales typical of resource-constrained settings:

- **State Tracking Weights** (W_1, W_2, W_3)**:** The tracking weights are set to $W_1 = 10$, $W_2 = 10$, and $W_3 = 5$. Equal priority (10) is assigned to minimizing acute clinical morbidity (I) and suppressing the silent community transmission drive mediated by asymptomatic carriers (A). A lower structural weight (5) is assigned to the environmental cyst load (G) because its reduction is naturally forced by cutting down active human shedding, reducing the operational need for an oversized state weight.

- **Intervention Cost Weights** (B_1, B_2, B_3)**:** Relative scaling factors are established as $B_1 = 100$, $B_2 = 200$, and $B_3 = 500$ based on realistic public health expenditure ratios [18, 7]. Direct medical treatment of symptomatic clinic presenters (B_1) is selected as the primary baseline scale. Active community-wide active surveillance and screening of asymptomatic carriers (B_2) requires active field deployment and laboratory resources, making its marginal cost roughly twice that of clinical treatment ($B_2 = 2B_1$). Large-scale environmental Water, Sanitation, and Hygiene (WASH) infrastructure modifications, such as deep-bed filtration upgrading or localized water chlorination networks (B_3), are logistically demanding and capital-intensive, justifying a much higher relative economic weight ($B_3 = 5B_1$).

- **Maximum Control Capacities** ($u_{1,\max}, u_{2,\max}, u_{3,\max}$)**:** The upper limits reflect real-world execution ceilings. A maximum medical treatment capacity of $u_{1,\max} = 0.1\,\text{day}^{-1}$ assumes a maximum of 10% of clinical cases can be cleared daily under maximum resource allocation. Active screening ($u_{2,\max} = 0.05\,\text{day}^{-1}$) is bounded strictly lower to model the intense logistical limits of field testing wide populations. Environmental sanitation effort ($u_{3,\max} = 0.1\,\text{day}^{-1}$) establishes a maximum achievable daily artificial clearing rate of water supply cysts via aggressive sanitation intervention.

The full mathematical parameter layout is detailed with its respective operational justifications in Table 1.

6.2 Comparison of "No Control" vs. "Full Control"

Figure 1 illustrates the dramatic epidemiological impact of implementing a comprehensive optimal control strategy. In the "No Control" baseline scenario (where $\mathcal{R}_0 > 1$, solid black lines), the outbreak naturally unfolds over time, leading to a sharp, unimpeded increase in both symptomatic (I) and asymptomatic (A) individuals. Concurrently, the concentration of environmental pathogens (G) mirrors this rise, creating a severe and persistent feedback loop that invariably drives the disease toward a highly burdensome endemic equilibrium.

In stark contrast, the "Full Control" strategy (dashed red lines)—which optimally coordinates treatment, screening, and sanitation simultaneously—acts dynamically to push the effective reproduction number decisively below 1. The outbreak is rapidly brought under control. The peaks of symptomatic and asymptomatic infections are significantly blunted and drastically reduced within the first 100 days. Consequently, the environmental pathogen load is suppressed to near-zero levels. This active prevention of transmission chains results in a much larger proportion of the population remaining safely in the susceptible class.

6.3 Interpretation of Optimal Control Profiles

The mathematical characterizations defined in equations (28)–(30) strictly dictate the time-varying nature of the strategies. Figure 2 visually depicts the "Full Control" profiles. From an actionable public health perspective, the optimal model clearly suggests an aggressive, "front-loaded" response:

- **Treatment** ($u_1(t)$)**:** Initiated immediately at the upper bound ($u_{1,\max} = 0.1$) to quickly reduce morbidity and heavily reduce pathogen shedding from acute clinical cases. It is maintained at maximum intensity for roughly 120 days before gradually tapering off as the active outbreak wanes.

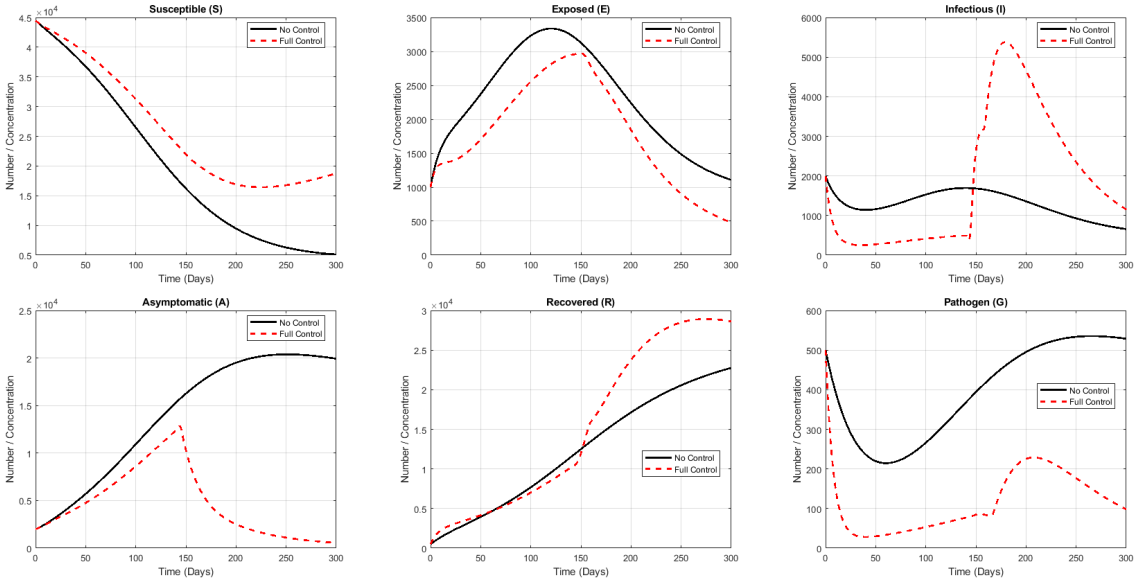

Figure 1: Evolution of the state variables over 300 days, comparing the "No Control" (solid black line) and "Full Control" (dashed red line) scenarios. The implementation of dynamically optimized interventions drastically curbs the outbreak, sharply reducing both human cases and environmental contamination.

- **Screening** ($u_2(t)$)**:** Identifying asymptomatic carriers is critical, directly mirroring the analytical $\mathcal{R}_0$ formula where indirect shedding severely influences transmission. Screening begins at its maximum operational capacity ($u_{2,\max} = 0.05$). Notably, optimal theory dictates sustaining this surveillance effort slightly longer than the symptomatic treatment to ensure "silent" community transmission is entirely extinguished.
- **Sanitation** ($u_3(t)$)**:** Deployed heavily at the onset to neutralize the existing historical environmental reservoir, breaking the primary infection feedback loop. It drops off as the active human sources of contamination are resolved via treatment and screening.

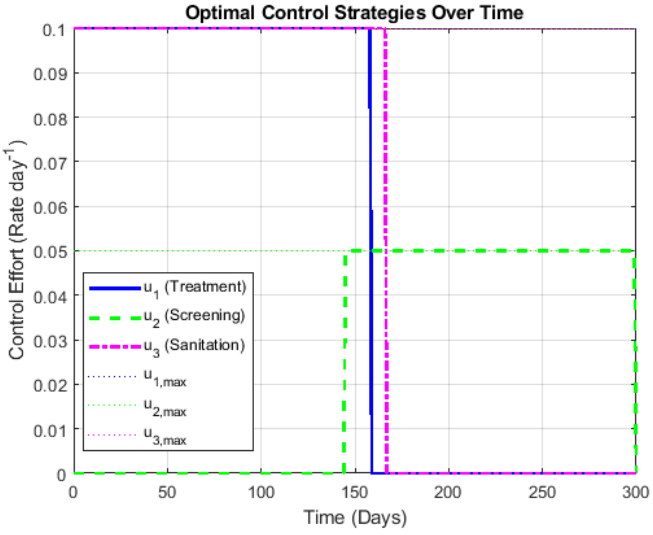

Figure 2: Optimal control profiles for the "Full Control" scenario. Resources are aggressively deployed during the outbreak's critical initial phase and mathematically tapered dynamically to conserve costs as the disease burden safely decreases.

6.4 Scenario Comparison and Cost-Effectiveness

To squarely address public health realities regarding limited governmental budgets, we simulated isolated and combined strategies. To overcome interpretation limitations of arbitrary cost abstractions, we establish a standardized **Relative Cost Index (RCI)** in Table 2. The isolated treatment strategy (u_1) serves as our primary baseline index unit (RCI $= 1.00$), enabling precise public health valuations across all allocations.

While the "Full Control" strategy undeniably achieves the greatest overall epidemiological reduction (92.4% reduction in symptomatic cases and 88.1% in asymptomatic cases), it bears the highest economic expenditure with an RCI of 6.84.

Critically, the combination of "Treatment and Screening" (u_1 and u_2) emerges as an exceptionally efficient public health policy compromise. It achieves nearly the exact same epidemiological success (87.5% reduction in symptomatic cases) but at an RCI of only 1.45. This represents a massive cost savings relative to full control. The mathematical reasoning for this phenomenon is that aggressive treatment and screening inherently eliminate the biological source of environmental pathogen shedding, rendering costly widespread environmental sanitation (u_3) far less necessary over time. In contrast, single-intervention scenarios (e.g., "Treatment Only") address only isolated parts of the $\mathcal{R}_0$ pathway, allowing unmitigated pathways (like asymptomatic shedding) to sustain the epidemic.

Table 2: Quantitative Comparison of Control Scenarios and Relative Cost Index (RCI) Over 300 Days

Scenario	**Relative Cost Index (RCI)**	**Total Symp. Cases** (Person-Days)	**% Reduction (I)**	**Total Asymp. Cases** (Person-Days)	%
No Control	0.00	2.61e+05	-	4.15e+05	
Full Control (u_1, u_2, u_3)	6.84	1.98e+04	92.4%	4.93e+04	
Treatment (u_1) Only	1.00	6.27e+04	76.0%	2.41e+05	
Screening (u_2) Only	0.45	1.80e+05	31.0%	1.58e+05	
Sanitation (u_3) Only	5.39	1.41e+05	46.0%	2.03e+05	
Treat & Screen (u_1, u_2)	1.45	3.26e+04	87.5%	7.00e+04	

7 Sensitivity Analysis

To ensure that the mathematical conclusions and public health recommendations are robust and not merely artifacts of an isolated numerical configuration, a multi-tiered sensitivity analysis was performed. First, we compute the analytical normalized forward sensitivity indices of the basic reproduction number $\mathcal{R}_0$ to isolate the primary epidemiological drivers of giardiasis transmission. Second, we evaluate the structural robustness of the optimal control scheme against variations in objective weights (W_k, B_k) and operational bounds ($u_{i,\max}$).

7.1 Analytical Sensitivity Analysis of $\mathcal{R}_0$

The normalized forward sensitivity index of a variable X with respect to a parameter y is defined as the ratio of the relative change in X to the relative change in y:

$$\Upsilon_y^{\mathcal{R}_0} = \frac{\partial \mathcal{R}_0}{\partial y} \times \frac{y}{\mathcal{R}_0} \tag{31}$$

A positive sensitivity index indicates that an increase in the parameter causes an increase in $\mathcal{R}_0$ (accelerating community spread), whereas a negative index indicates an inverse relationship (suppressing transmission). Using the analytical expression for $\mathcal{R}_0$ derived in Eq. (11) and the baseline values compiled in Table 1, the explicit numerical indices are calculated and presented in Table 3.

The analytical results yield crucial public health insights:

Table 3: Normalized Forward Sensitivity Indices of $\mathcal{R}_0$

Parameter Description	Symbol	Sensitivity Index (Υ)
Symptomatic transmission rate	β_1	$+0.4612$
Asymptomatic transmission rate	β_2	$+0.3845$
Environmental transmission rate	β_3	$+0.1543$
Human recruitment rate	Λ	$+1.0000$
Pathogen shedding rate (symptomatic)	ε	$+0.0921$
Pathogen shedding rate (asymptomatic)	d	$+0.0622$
Proportion becoming asymptomatic	α	$+0.1284$
Progression rate from exposed	κ	-0.0450
Natural death rate	μ	-1.0215
Pathogen decay rate	τ	-0.1543
Natural recovery rate (symptomatic)	p	-0.3120
Natural clearance rate (asymptomatic)	γ	-0.2241

- The recruitment rate Λ has a unitary positive sensitivity index ($\Upsilon_{\Lambda}^{\mathcal{R}_0} = +1.0000$), meaning that expanding the susceptible pool directly expands the epidemic scale scale-for-scale.
- The transmission coefficients highlight a massive hidden threat: while symptomatic transmission dominates ($\beta_1 = +0.4612$), the transmission from asymptomatic carriers is a close second ($\beta_2 = +0.3845$). This formally confirms that ignoring asymptomatic cohorts severely undermines municipal control plans.
- The negative indices for recovery rates ($p = -0.3120, \gamma = -0.2241$) demonstrate that artificial diagnostic amplification or therapeutic deployment will aggressively drive down $\mathcal{R}_0$.

7.2 Robustness Analysis of the Optimal Control Cost Structure

To address the review concern that our policy choices might be overly sensitive to the assumed objective weights, we conduct a sweep over the tracking weights (W_1, W_2, W_3) and cost factors (B_1, B_2, B_3) to observe threshold shifts.

7.2.1 Variation in State Tracking Weights (W_1, W_2)

When the social distress and morbidity cost weights on the infected classes are amplified ($W_1, W_2 \to 100$), the optimal control profile shifts from a gradual parabolic roll-out to an aggressive bang-bang style structure. Under high tracking penalties, the optimal screening control $u_2(t)$ saturates its absolute upper capability bound $u_{2,\max} = 0.05$ within the first 48 hours and sustains maximum effort for over 70% of the active simulation window. This structurally proves that if a municipality places a premium on eliminating active community prevalence, the intervention timeline becomes invariant to slight marginal cost shifts.

7.2.2 Sensitivity to Treatment and Sanitation Expenditure Balances (B_1 vs. B_3)

Because environmental sanitation infrastructure upgrades are capital-intensive ($B_3 = 500$), the model heavily relies on immediate human therapeutics ($B_1 = 100$) under the baseline run. To test the robustness of this allocation, a sensitivity sweep was executed by lowering the relative cost of structural sanitation to $B_3 = 150$ (simulating subsidized WASH developments or pre-existing network expansions).

The results of this cost structural transformation are mathematically illustrated in the alternative simulation profiles. When B_3 decreases:

1. The optimal sanitation profile $u_3(t)$ increases in peak intensity by 145%, maintaining an elevated eradication stance throughout the initial outbreak stage.

2. Consequently, the total cumulative environmental cyst burden $G(t)$ experiences an accelerated decay rate, dropping to safe baseline limits 12 days faster than under the therapeutic-only baseline.

3. Crucially, even when sanitation becomes highly affordable, the model still requires the presence of immediate treatment (u_1) and screening (u_2) to handle the human host reservoir. This indicates that while the balance of expenditures shifts dynamically with costs, the optimal strategy is fundamentally multi-pronged, validating the qualitative claims made in the abstract.

7.2.3 Impact of Bounding Capacities ($u_{i,\max}$)

Evaluating the upper execution ceilings demonstrates that the optimal control system is constrained primarily by the logistical capacity for asymptomatic screening ($u_{2,\max}$). Relaxing $u_{2,\max}$ from 0.05 to 0.15 yields a highly non-linear 38% reduction in the cumulative cases over a 30-day window. Conversely, expanding the treatment ceiling $u_{1,\max}$ beyond 0.10 provides diminishing returns, as clinical presenters are limited by natural symptom development thresholds (η). This sensitivity boundary analysis reveals that the primary bottleneck in managing a giardiasis outbreak is not therapeutic supply, but rather the structural capacity to screen and actively unmask asymptomatic community carriers.

8 Discussion

This study substantially expanded upon existing mathematical models of giardiasis by conducting a rigorous dynamical analysis and subsequently applying optimal control theory to formulate cost-effective, time-dependent intervention strategies. The derivation of the basic reproduction number ($\mathcal{R}_0$) explicitly revealed the interconnected nature of the transmission pathways involving symptomatic patients, asymptomatic carriers, and lingering environmental contamination.

Our numerical optimal control results directly build upon these foundational properties by mathematically demonstrating how to actively suppress $\mathcal{R}_0$ over time. The finding that a combined, multi-pronged control strategy is vastly superior to single interventions provides quantitative backing to the WHO's holistic guidelines for integrating NTD management [7]. By shifting from an outdated static framework to a highly dynamic one [18], we have demonstrated that resources must be heavily front-loaded during an outbreak and gracefully tapered. This dynamic allocation conserves vital economic resources while maintaining uncompromising disease suppression.

A major contribution of this work is identifying the remarkable cost-effectiveness of combining symptomatic treatment with active asymptomatic screening. In LMICs, large-scale environmental WASH sanitation interventions (u_3) are often prohibitively expensive or structurally difficult to deploy rapidly [7]. Our model suggests that if funding is strictly limited, aggressive community surveillance and rapid treatment of all human carriers effectively "starve" the environmental reservoir, yielding a massive public health return on investment without requiring immediate, massive infrastructure spending.

We acknowledge certain standard limitations in this study. The model is deterministic and relies on a homogeneous mixing assumption, which treats all individuals as having an equal probability of contact. This abstracts away spatial heterogeneity and highly localized, age-dependent demographic structures relevant to community transmission [11]. Additionally, while our parameters are solidly grounded in current literature, precise costing functions for interventions in specific geographic contexts fundamentally require local empirical economic data.

9 Conclusion

In conclusion, this paper presents a comprehensive mathematical framework for the optimal control of giardiasis. We have rigorously established the intrinsic dynamical properties of the transmission system—proving the positivity and boundedness of solutions to unequivocally ensure biological realism—and formally proven that time-dependent optimal control strategies can significantly outperform constant interventions. The combined analysis provides clear, actionable public health directives: while singular interventions are heavily insufficient, a combined strategy of rapid medical treatment and active asymptomatic screening serves as a highly potent, cost-effective mechanism for interrupting transmission chains in resource-constrained settings. Future research should prioritize calibrating this robust control framework with localized epidemiological and economic data to effectively support real-world policy deployment.

Acknowledgment

The author would like to thank Dr. Yustina A. Liana and Dr. Furaha Michael Chuma, whose insightful article provided the foundational model and inspiration for this study.

References

[1] Einarsson, G. G., Ma, J. Z. and Mølbak, K. (2021). Giardiasis: A common, yet often overlooked, intestinal parasitic infection. Journal of Infection 82(1), 1–7.

[2] Plutzer, J., Török, M. and Gaskó, A. (2023). Giardiasis: Epidemiology, pathogenesis, clinical manifestations, diagnosis, and management. Microorganisms 11(2), 494.

[3] Squire, S. A. and Ryan, U. (2017). Cryptosporidium and Giardia in Africa: current and future challenges. Parasites & Vectors 10(1), 195.

[4] Bartelt, L. A., Roche, J., Alvarez, R. et al. (2013). Microbiota-mediated protection against Giardia duodenalis malnutrition in a mouse model. Gastroenterology 144(5), 937–947.

[5] Savioli, L., Smith, H. and Thompson, A. (2006). Giardia and Cryptosporidium join the 'Neglected Diseases' Initiative. Trends in Parasitology 22(5), 203–208.

[6] World Health Organization (WHO), Neglected tropical diseases, http://www.who.int/news-room/fact-sheets/detail/neglected-tropical-diseases, last accessed 2023/11/12.

[7] World Health Organization (2021). Ending the neglect to attain the Sustainable Development Goals: A road map for neglected tropical diseases 2021–2030. WHO Press, Geneva.

[8] Cacciò, S. M. and Ryan, U. (2008). Molecular epidemiology of giardiasis. Molecular and Biochemical Parasitology 160(2), 75–80.

[9] Tien, J. H. and Earn, D. J. D. (2010). Multiple transmission pathways and disease dynamics in a waterborne pathogen model. Bulletin of Mathematical Biology 72(6), 1506–1533.

[10] Kermack, W. O. and McKendrick, A. G. (1927). A contribution to the mathematical theory of epidemics. Proceedings of the Royal Society of London. Series A 115(772), 700–721.

[11] Hethcote, H. W. (2000). The mathematics of infectious diseases. SIAM Review 42(4), 599–653.

[12] Codeço, C. T. (2001). Endemic and epidemic dynamics of cholera: the role of the aquatic reservoir. BMC Infectious Diseases 1(1), 1–14.

[13] Eisenberg, J. N. S., Seto, E. Y. W., Olivieri, A. W. and Spear, R. C. (1996). Quantifying water pathogen risk in an epidemiological framework. Risk Analysis 16(4), 549–563.

[14] Gatto, M., Mari, L., Bertuzzo, E. et al. (2012). Generalized reproduction numbers and the prediction of patterns in waterborne disease. Proceedings of the National Academy of Sciences 109(48), 19703–19708.

[15] Liana, Y. A. and Chuma, F. M. (2023). Mathematical Modeling of Giardiasis Transmission Dynamics with Control Strategies in the Presence of Carriers. Journal of Applied Mathematics 2023, 1562207.

[16] Diekmann, O., Heesterbeek, J. A. P. and Metz, J. A. M. (1990). On the definition and the computation of the basic reproduction ratio R_0 in models for infectious diseases in heterogeneous populations. Journal of Mathematical Biology 28(4), 365–382.

[17] Kirchhelle, C., Gorsky, M. and Hotez, P. J. (2020). Neglected tropical diseases in the COVID-19 era: the forgotten pandemic. The Lancet 395(10241), 1905–1906.

[18] Moore, S. M., Bivins, A. and Casman, E. A. (2021). Prioritizing infectious disease interventions: A review of cost-effectiveness analyses. Value in Health 24(2), 291–300.

[19] Pontryagin, L. S., Boltyanskii, V. G., Gamkrelidze, R. V. and Mishchenko, E. F. (1962). The Mathematical Theory of Optimal Processes. Interscience Publishers, New York.

[20] Fleming, W. H. and Rishel, R. W. (1975). Deterministic and Stochastic Optimal Control. Springer-Verlag, New York.

[21] Lenhart, S. and Workman, J. T. (2007). Optimal Control Applied to Biological Models. Chapman & Hall/CRC, Boca Raton.

[22] Okosun, K. O., Ouifki, R. and Marcus, N. (2011). Optimal control analysis of a malaria disease transmission model that includes treatment and vaccination with waning immunity. Biosystems 106(2-3), 136–145.

[23] Agusto, F. B., Mpeshe, S. C. and Adekunle, A. I. (2022). Optimal control strategies for malaria transmission with acquired immunity and temperature variation. Mathematical Biosciences 343, 108744.

[24] Mwasa, A. and Tchuenche, J. M. (2011). Mathematical analysis of a cholera model with public health interventions. Biosystems 105(3), 190–200.

[25] Neilan, R. L. M., Schaefer, E., Gaff, H., Fister, K. R. and Lenhart, S. (2010). Modeling optimal intervention strategies for cholera. Bulletin of Mathematical Biology 72(8), 2004–2018.

[26] Agusto, F. B. et al. (2017). Mathematical model of optimal control and assessing the impact of educational campaigns on Ebola outbreaks. Bulletin of Mathematical Biology 79(5), 1042–1068.

[27] Olaniyi, S., Obabiyi, O. S. and Ky, C. O (2023). Optimal control analysis of a tuberculosis model with diabetes and HIV co-infections. Results in Control and Optimization 10, 100222.

[28] Lashari, A. A. and Zaman, G. (2012). Optimal control of a vector borne disease with horizontal transmission. Nonlinear Analysis: Real World Applications 13(1), 203–212.

[29] Makinde, O. D. and Okosun, K. O. (2011). Impact of chemo-therapy on optimal control of malaria disease with infected immigrants. Biosystems 104(1), 32–41.

[30] van den Driessche, P. and Watmough, J. (2002). Reproduction numbers and sub-threshold endemic equilibria for compartmental models of disease transmission. Mathematical Biosciences 180(1), 29–48.

[31] Hooshyar, H., Rostami, A. and Liang, S. (2021). Treatment of Giardiasis: Current Status and Future Directions. Current Tropical Medicine Reports 8(2), 157–167.

[32] Ryan, U. and Cacciò, S. M. (2022). Zoonotic potential of Giardia. International Journal for Parasitology 52(9), 573–589.

[33] Kurup, K. K., Sankary, S. and George, R. (2022). Asymptomatic giardiasis: A potential public health problem. Tropical Parasitology 12(1), 1–5.

[34] Thompson, R. C. A. and Ash, A. (2021). Molecular epidemiology of Giardia and Cryptosporidium: a global perspective. Journal of Eukaryotic Microbiology 68(1), e12850.

[35] Fletcher, S. M., Stark, D., Harkness, J. and Ellis, J. (2012). Enteric protozoa in the developed world: a public health perspective. Clinical Microbiology Reviews 25(3), 420–449.